Integration of Inductively Coupled Power Transfer and Hybrid Energy Storage System: A Multiport Power Electronics Interface for Battery-Powered Electric Vehicles

Matthew McDonough, *Member, IEEE*

***Abstract*—Detailed in this paper is a multiport power electronics interface which serves as an energy router for on-board electric and plug-in hybrid electric vehicles with inductively coupled power transfer (ICPT) and hybrid energy storage systems (HESS). The existing body of literature on HESSs lacks a unified controller and modular, flexible structure as well as integration of ICPT. In battery/ultracapacitor systems, this leads to piece-meal control of sources resulting in battery currents which are not fully decoupled from high-frequency/high-magnitude current and ultra-capacitor (UC) state of charge (SoC) not being properly controlled. A central controller is proposed in this paper which completely decouples the battery from both high-frequency and high-magnitude current, controls the SoC of the UCs, and models the SoC of the UCs in the stability analysis of the system. This system is particularly useful for online charging of HEVs in highway-type applications where ICPT pulse charging will be present. Solving the challenges of pulse charging will bring ICPT technology one step closer to widespread integration which has the potential to greatly reduce societies' dependence on fossil fuel. Simulation and experimental results verify the feasibility of the proposed techniques.**

***Index Terms*—Hybrid energy storage system (HESS), inductively coupled power transfer (ICPT), multiport power electronics, wireless power transfer (WPT).**

I. Introduction

THERE exists a growing focus on the reduction of fossil fuel usage due to concerns about pollution, geopolitical conflicts, and climate change. Transportation accounts for 28% of the energy usage in the United States [1] and that fuel is almost exclusively derived from fossil fuel. The introduction of electric vehicles (EVs) and hybrid electric vehicles (HEVs) has the potential to reduce the consumption of fossil fuel and their adverse effects [2]. However, range anxiety and high cost of batteries are preventing the battery powered EVs (BEVs) from dominating the market place.

In order to solve these challenges, there has been much focus on battery technology. Work is under way to produce batteries which have larger capacity per unit weight/volume, the ability to discharge more quickly, and estimate state of charge (SoC) more accurately [3]–[5]. Quick charging of these batteries is also a growing area of research [6]–[8]. It is thought that if a consumer can charge the vehicle as quickly as one can fill up a gas tank, then the range anxiety will diminish. All of these technologies are critical for improving the range of the BEV; however, to become par with combustion vehicles, the specific energy storage will have to increase by at least an order of magnitude and the charging time will need to drop to 5–10 min.

It is with these boundary conditions that the idea of charging while driving using inductively coupled power transfer (ICPT) has been proposed [9]–[12]. ICPT is a method with which to transfer power across a physical gap between a primary and a secondary resonating coil. The primary side inverter will inject an alternating current to the primary side winding, typically after creating a resonating tank using capacitors and sometimes additional inductors. A portion of the AC electro-magnetic field (EMF) created by the primary transmitter will pass through the coil of the secondary side receiver which also typically has a resonating tank. This results in an ac voltage due to Faraday's law, which is processed by the secondary side power electronics and applied to the load. ICPT technology is maturing for stationary applications with start-up companies producing add-on components for BEVs [13], [14].

When ICPT is applied in a moving arena, new challenges arise. Particularly, pulse charging (which is a result of charging in motion with ICPT) of batteries is detrimental to the lifespan of the batteries. While the concept of pulse charging while driving has many benefits, it also puts a large burden on the power electronics and the on-board battery. It has been shown that high-magnitude and high-frequency currents imposed on the battery will reduce the battery life [15]–[19]. For similar applications, hybrid energy storage systems (HESS) have been proposed by many authors [20]–[29]. HESS have at least two sources of energy storage. Usually one has higher specific power and one has higher specific energy. Typical HESS combinations are: battery, ultra-capacitor (UC); fuel-cell, battery; fuel-cell, UC; and many other combinations.

A battery, UC HESS was developed for automotive systems in [17] which uses a heuristic saturation algorithm to keep the battery current below a preset maximum. This method limits the peak currents on the battery in the experimental results given. This provides a practical solution to keep the battery current below a desired threshold. However, stability cannot be

Manuscript received December 12, 2014; revised February 20, 2015; accepted March 12, 2015. Date of publication April 13, 2015; date of current version July 10, 2015. Recommended for publication by Associate Editor S. Williamson.

The author is with the Department of Electrical Engineering, The University of Texas at Dallas, Dallas, TX 75080 USA (e-mail: matthew.mcdonough@utdallas.edu).

Color versions of one or more of the figures in this paper are available online at http://ieeexplore.ieee.org.

Digital Object Identifier 10.1109/TPEL.2015.2422300

guaranteed with this nonlinear method of control. Additionally, a separate controller will have to be added to keep the UCs within a reasonable range, otherwise the proposed control strategy will eventually discharge the UCs. Also, the battery is still exposed to high-frequency current components.

In [30] (battery, UC system), the measured battery current was used as a reference for the UC controller. Average current and peak current from the battery is reduced in this application. High-frequency and high-magnitude currents can still be present at the battery terminal, though. This is because the battery current controller is directly responsible for maintaining the dc bus and the UC current controller will not begin to aid until the current magnitude exceeds a predefined set point. Similar to the previous work, an additional controller is necessary to maintain the UC SoC.

A combustion engine, battery, UC system is described in [21]. In this paper, the lowest frequency power is derived from the combustion engine, the midband power is taken from the battery, and the high-frequency components come from the UC. In this paper, the effects of such a power split system is studied. In [31], the same authors have results from a battery, UC system which shows part of the power coming from the battery and part from the UCs. The magnitude of the battery current is greatly reduced, but the high-frequency response is still present.

Finally, Ortuzar *et al.*[32] shows a full power battery, UC HESS integrated into an electric vehicle. This system uses the UC SoC as a fundamental part of the control by varying the desired SoC based on the speed of the vehicle. Similar to other methods though, the UCs are only used to reduce the peak demand on the batteries. Therefore, there is unnecessary power cycling in the batteries with high frequency which will degrade the batteries faster.

While this is not an exhaustive compilation of HESS research, there is a noticeable gap in the research. First, the SoC of the UC should be included in the closed loop control system. Second, the battery should not be exposed to excessive charge/discharge cycles, especially due to high-frequency current requirements of the dc bus. Third, these systems are generally three port systems: battery, UC, load. A modeling approach for an arbitrary n-port system is desirable. Finally, ICPT should be added to the HESS to determine its effect on the system. It is the objective of this paper to fill that gap by providing a modeling technique for multiport converters which is both modular, expandable, and fully decouples the high-magnitude/high-frequency current components from the battery while also easily adapting to unique inputs such as ICPT.

In Section II, ICPT's role in the proposed multiport converter is discussed and the key objectives of this paper are described. In Section III, the approach to modeling a multiport converter with closed loop controllers is presented. Simulation results are presented in Section IV and experimental results are presented in Section V. A final discussion of the system and results is given in Section VI.

II. Introduction to MPEI and ICPT

Multiport power electronics interface (MPEI) is a concept that is ideally suited for BEV applications, especially applications which include HESSs and ICPT systems. MPEI is a structure which uses a unified controller to control multiple converters which typically share a common dc bus. With this concept, the current of each source can be manipulated independently. This allows the integration of a wide range of optimization criteria such as efficiency, reliability, and cost of operation; among others. Applications of MPEI are described for stationary vehicle charging in [10]; microgrids in [33], [34]; and BEVs in [10], [35].

In order to charge a vehicle while it is in transit, there are two separate scenarios which might occur. At any given time, the vehicle will likely either be stopped (at red lights, stop signs, etc.) or moving at a high rate of speed (i.e., highway applications or in-between stops). In [10], it is shown that the battery pack of a commercially available BEV could be reduced by 66% by charging at moderate (20 kW) levels at stand still in urban environments. This resulted in a 13% reduction of vehicle weight and indefinite extension in driving range (however this is only for urban environments). This results in a substantial reduction in cost of a BEV. In [36], this idea was extended to the highway environment. It was shown that with peak charging levels of 60 kW, a series of 1-m-wide square transmitter pads could pulse charge the BEV to provide continuous motion for a light vehicle traveling at 60 mph. In this study, there were two meters separating each coil on the highway system.

In this application of MPEI, ICPT is the primary source of energy into the system. The addition of ICPT to the multiport converter is the key which will allow continuous transportation in a BEV with minimal on-board energy storage in either urban or high speed environments. Additionally, the philosophy of the unified controller in MPEI provides a unique ability to control the power flow within the MPEI. This is critical for maintaining the SoC of the UCs and the battery while continuously providing power to the load. The topology for MPEI coupled with ICPT and a HESS is given in Fig. 1, where the MPEI is primarily made of a series of bidirectional single-legged switching dc–dc converters.

III. System Modeling

A. Modeling a Single DC–DC Converter

A single-legged switching dc–dc converter can be modeled using the generalized averaged model proposed in [37]. With this technique, the state space model of the dc–dc converter is given as

$$\begin{aligned} \dot{I}_l &= \frac{1}{L} \times (D \times V_{\rm dc} - V_c) \\ \dot{V}_c &= \frac{1}{C} \times (I_l - I_o) \end{aligned} \tag{1}$$

Here, I_l, L, D, $V_{\rm dc}$, V_c, C, and I_o are the inductor current, inductance, top switch duty cycle, dc bus voltage, output terminal capacitor voltage, capacitance, and output terminal current, respectively.

With the state space model of the switching converter, a controller can be added to stabilize the system. In this application, cascaded PI controllers of the type shown in Fig. 2 are used;

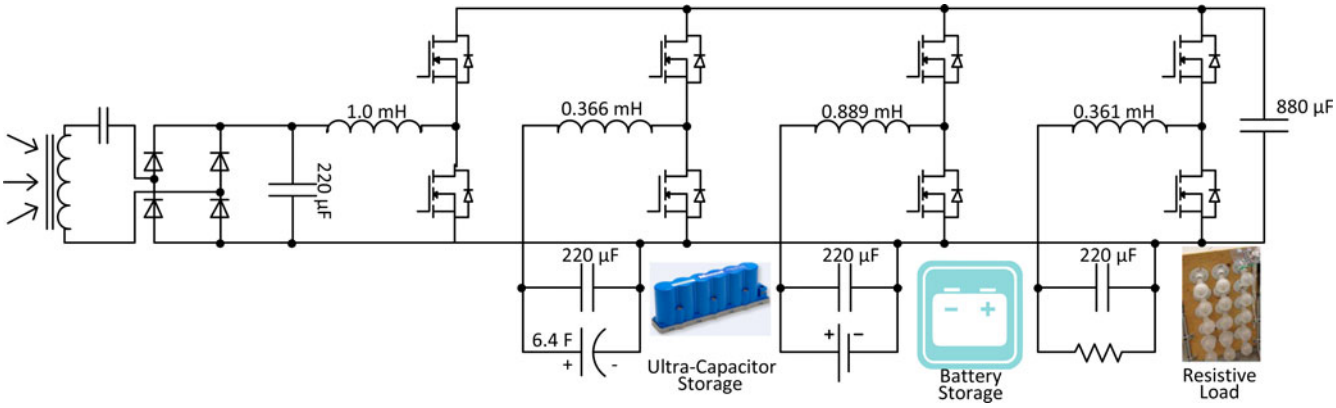

Fig. 1. Topology for BEV MPEI which has ICPT system.

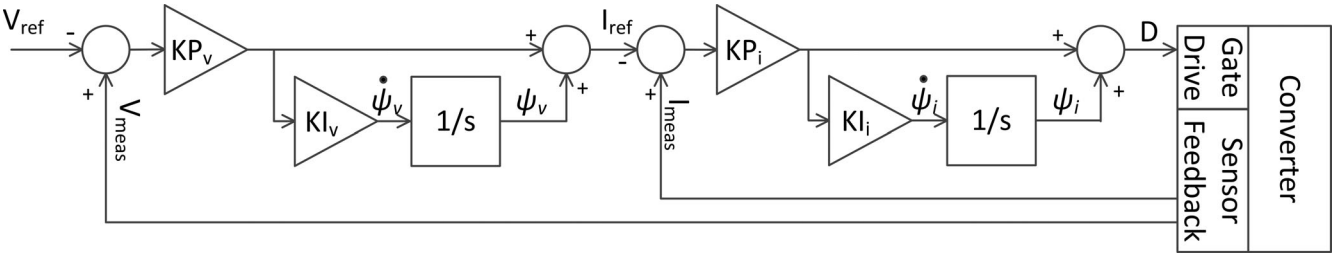

Fig. 2. Cascade voltage-current controller.

however, the modeling approach is valid for any manner of linear controller.

The state space average model for the cascaded PI controllers of Fig. 2 is given in (2) where the output of the system is the duty cycle given as

$$\begin{aligned}\dot{\Psi}_V &= (V_{\text{meas}} - V_{\text{ref}})kp_V\, ki_V \\ \dot{\Psi}_I &= [(V_{\text{ref}} - V_{\text{meas}})kp_V - \Psi_V + I_l]kp_I ki_I \qquad (2)\\ D &= [(V_{\text{ref}} - V_{\text{meas}})kp_V - \Psi_V + I_l]kp_I + \Psi_I. \qquad (3)\end{aligned}$$

By combining (1)–(3), the state space model of one dc–dc converter can be obtained which is given as

$$\begin{aligned}\dot{\Psi}_V &= (V_{\text{meas}} - V_{\text{ref}})kp_V\, ki_V \\ \dot{\Psi}_I &= [(V_{\text{ref}} - V_{\text{meas}})kp_V + I_l - \Psi_V]kp_I ki_I \\ \dot{I}_l &= \frac{1}{L}\{[(V_{\text{ref}} - V_{\text{meas}})kp_V\, kp_I + I_l kp_I \\ &\quad - \Psi_V kp_I + \Psi_I]V_{dc} - V_c\} \\ \dot{V}_c &= \frac{1}{C}(I_l - I_o). \qquad (4)\end{aligned}$$

Finally, this model can be split into the small signal model and the large signal components. In small signal modeling, the common practice of neglecting any Δ^2 value is utilized to linearize the system. Also, the system is assumed to be in steady-state operation. The resulting set of state space equations is given as

$$\begin{aligned}\Delta\dot{\Psi}_V &= (\Delta V_{\text{meas}})kp_V\, ki_V \\ \Delta\dot{\Psi}_I &= [(-\Delta V_{\text{meas}})kp_V + \Delta I_l - \Delta\Psi_V]kp_I ki_I \\ \Delta\dot{I}_l &= \frac{1}{L}\{[(-\Delta V_{\text{meas}})kp_V\, kp_I + \Delta I_l kp_I \\ &\quad - \Delta\Psi_V kp_I + \Delta\Psi_I]\hat{V}_{dc} - \Delta V_c \\ &\quad + \Delta V_{dc}\hat{\Psi}_I\} \\ \Delta\dot{V}_c &= \frac{1}{C}(\Delta I_l - \Delta I_o) \qquad (5)\end{aligned}$$

At this point, it becomes beneficial to stabilize the individual converters by choosing kp and ki gains for individual converters. The results are shown in Section IV.

B. DC Bus Interaction

The interaction between each dc–dc converters appears on the dc bus and so another differential equation must be derived for the dc bus capacitor voltage. This equation is shown in (6), where D_n and I_n represent the duty cycle and current of the nth dc–dc converter

$$\dot{V}_{\text{dc}} = \frac{1}{C_{\text{dc}}}[-D_1 I_1 - D_2 I_2 - D_3 I_3 + \cdots]. \qquad (6)$$

If the small signal analysis of the previous section is employed on this equation, (6) becomes

$$\begin{aligned}\Delta\dot{V}_{dc} = \frac{1}{C_{dc}}\sum_{n=0}^{m}\{&[(-\Delta V_{\text{meas},n})kp_{V,n}kp_{I,n} \\ &+\Delta I_{l,n}kp_{I,n} - \Delta\Psi_{V,n}kp_{I,n} + \Delta\Psi_{I,n}]\hat{I}_{l,n} \\ &+\hat{\Psi}_{I,n}\Delta I_{l,n} + \hat{\Psi}_{I,n}\hat{I}_{l,n}\}. \qquad (7)\end{aligned}$$

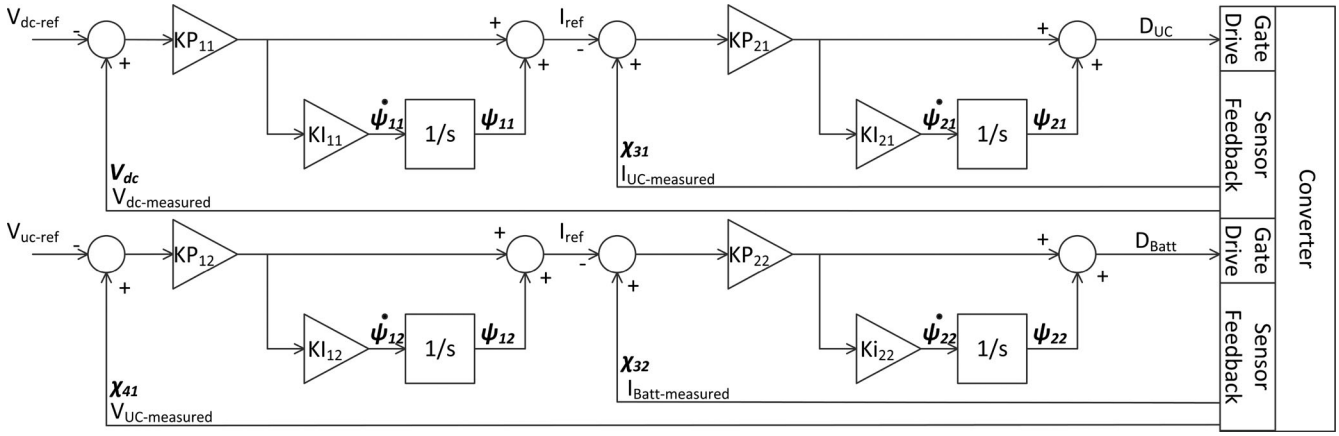

Fig. 3. Battery/ultra-capacitor controller.

Note that the last term in (7) does not include any small signal components. This term will disappear however because it represents the sum of the steady-state currents on the capacitor node. For the system to be in a steady-state condition, the sum of the steady-state currents on the capacitor must be equal to zero, or in other words, $\sum_{n=0}^{m} \hat{\Psi}_{I,n}\hat{I}_{l,n} \equiv 0$. This condition will be forced by the dc bus controller.

C. Battery-UC System

Since the system modeling technique is completed, the only step left is to assign $V_{\rm meas}$ and $V_{\rm ref}$ to each cascaded PI controller. $I_{\rm meas}$ is always the measured inductor current for the switching leg in which the output of the controller (which is the duty cycle) is applied and $I_{\rm ref}$ is always the output of the voltage controller for that particular converter. Since the UC has much better charge/discharge efficiency than the battery and since it has the ability to withstand more frequent charge/discharge cycles then the battery, it is appropriate to have the UC control the dc bus. Therefore, $V_{\rm meas}$ and $V_{\rm ref}$ in the UC controller are the measured dc bus voltage and the reference dc bus voltage, respectively.

Since the batteries' main function is to provide the low-frequency power, a low-pass filtered version of the UC current seems to be an appropriate current reference for the battery. If $V_{\rm meas}$ and $V_{\rm ref}$ for the battery is the measured UC voltage and desired UC voltage then a single controller can both provide the low-frequency power requirements for the load and maintain the UC SoC. This control diagram is shown in Fig. 3.

D. ICPT Terminal

The next step is to add the ICPT terminal. The resonant frequency of the ICPT terminal is typically higher than the switching frequency of the dc–dc converters. In this application, the resonant frequency is five times the switching frequency of the dc–dc converters. Additionally, the dynamics of the ICPT system (i.e., the ring-up from zero current to maximum current resonating in the secondary coil, for example) is faster than the controller's bandwidth. Therefore, after rectification, a filter will have to be added to reduce the bandwidth of the ICPT terminal. The filter is placed around the point labeled $V_{\rm meas}$ in Fig. 4. As the bandwidth of the ICPT terminal is so high and the nature of the charge-while-driving scenario is pulse charging, a step input is an appropriate way to model the current from the ICPT terminal.

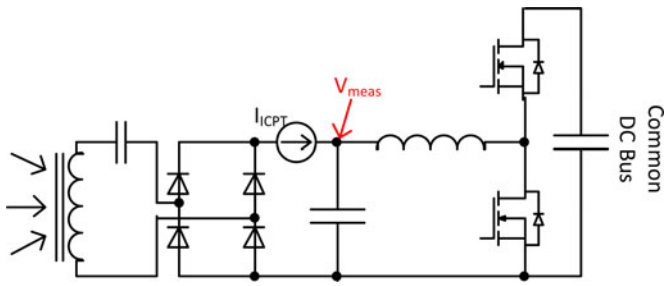

Fig. 4. ICPT terminal topology.

In the ICPT system, the output voltage (labeled $V_{\rm meas}$ in Fig. 4) is critical for efficiency and maximum power transfer of the ICPT system. If ICPT primary is transferring power to the secondary, the voltage of that terminal will tend to rise. The controller will be used to keep that terminal at the desired voltage thus drawing power into the MPEI. $V_{\rm meas}$ for the ICPT terminal is labeled in Fig. 4 and $V_{\rm ref}$ is the desired reference voltage for this point. That will most likely be the voltage which has the highest efficiency for the given topology.

E. Load Terminal

The load terminal for an EV will typically be a multiphase motor. A three-phase model has been added into an MPEI as shown in [33]. For simplicity, the load in this case is a dc resistive load. Therefore, similar to the ICPT terminal, $V_{\rm meas}$ and $V_{\rm ref}$ are the measured load voltage and reference load voltage.

F. Additional Terminals

Additional terminals can be added as well. Most terminals which act primarily as a load or which will harvest energy

TABLE I
ON-BOARD BEV MPEI CONTROLLER GAINS AND DOMINANT POLE

Controller	kp_V	ki_V	kp_I	ki_I	Dominant Pole
UCs	0.5	400	−10	−1500	−518.5
Battery	2.5	0.80	−10	−1500	−0.800
Load	−0.4	−35.7	−10	−2000	−36.43
ICPT	−0.4	−35.7	−10	−2000	−36.43

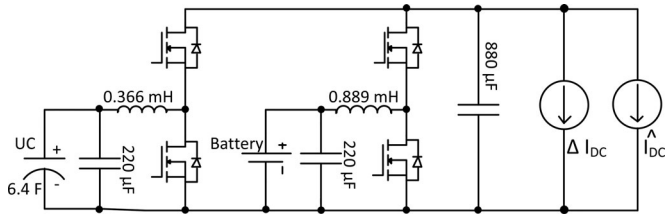

Fig. 5. Cascaded battery-UC system with dc bus load.

TABLE II
POLE LOCATIONS FOR CASCADED BATTERY-UC SYSTEM

	DC Bus Load Current	
Pole #	1 A (300 W)	8 A (2.4 kW)
	Poles	
1	-8.2×10^6	-8.2×10^6
2	-3.4×10^6	-3.4×10^6
3 & 4	-1.5×10^6	-1.5×10^6
5 & 6	$-111\pm274j$	$-124\pm268j$
7 & 8	$-0.20\pm0.53j$	$-0.20\pm0.53j$

whenever it is available (like the ICPT terminal) will most likely use the terminal voltage as the feedback. If additional energy storage terminals are added, a cascaded series of controllers can be used. For example, a Fuel cell's voltage controller might use the battery terminal voltage as the feedback, while the battery voltage controller uses the UC voltage as the feedback and the UC controller uses the dc bus voltage as the feedback.

IV. MODELING AND SIMULATION RESULTS

In order to verify the validity of the theoretical modeling and stability of the overall system, results from model simulation using MATLAB and the circuit simulation using PLECS is included in this section.

A. Single DC–DC Converter Modeling Results

Each dc–dc controller was modeled using the method developed in Section III-A. For individual controller modeling, the dc bus was considered fixed and the current direction was assumed to be flowing to the source/sink. Therefore, the converter was modeled in a buck-type operation. The values of the control parameters, kp and ki, and the dominant poles are given in Table I. The system is considered stable if all the poles are in the left-half plane of the s-domain which was the case for each dc–dc converter.

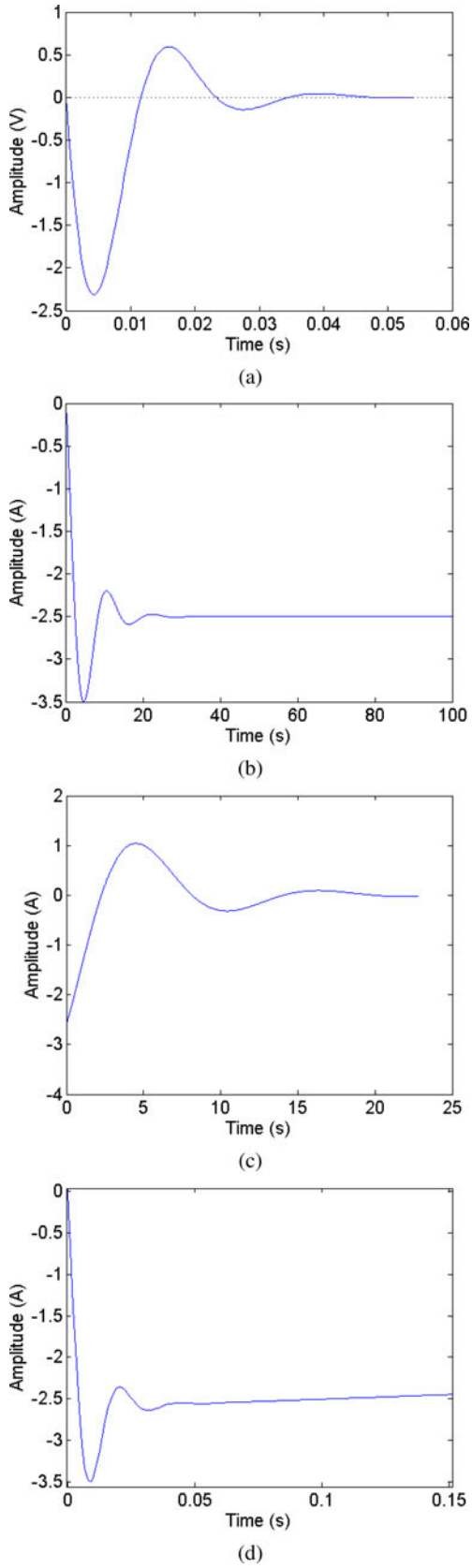

Fig. 6. Small Signal response in Battery - UC system to dc bus load step transients. (a) dc bus voltage; (b) Battery current; (c) UC current; (d) UC current (zoomed).

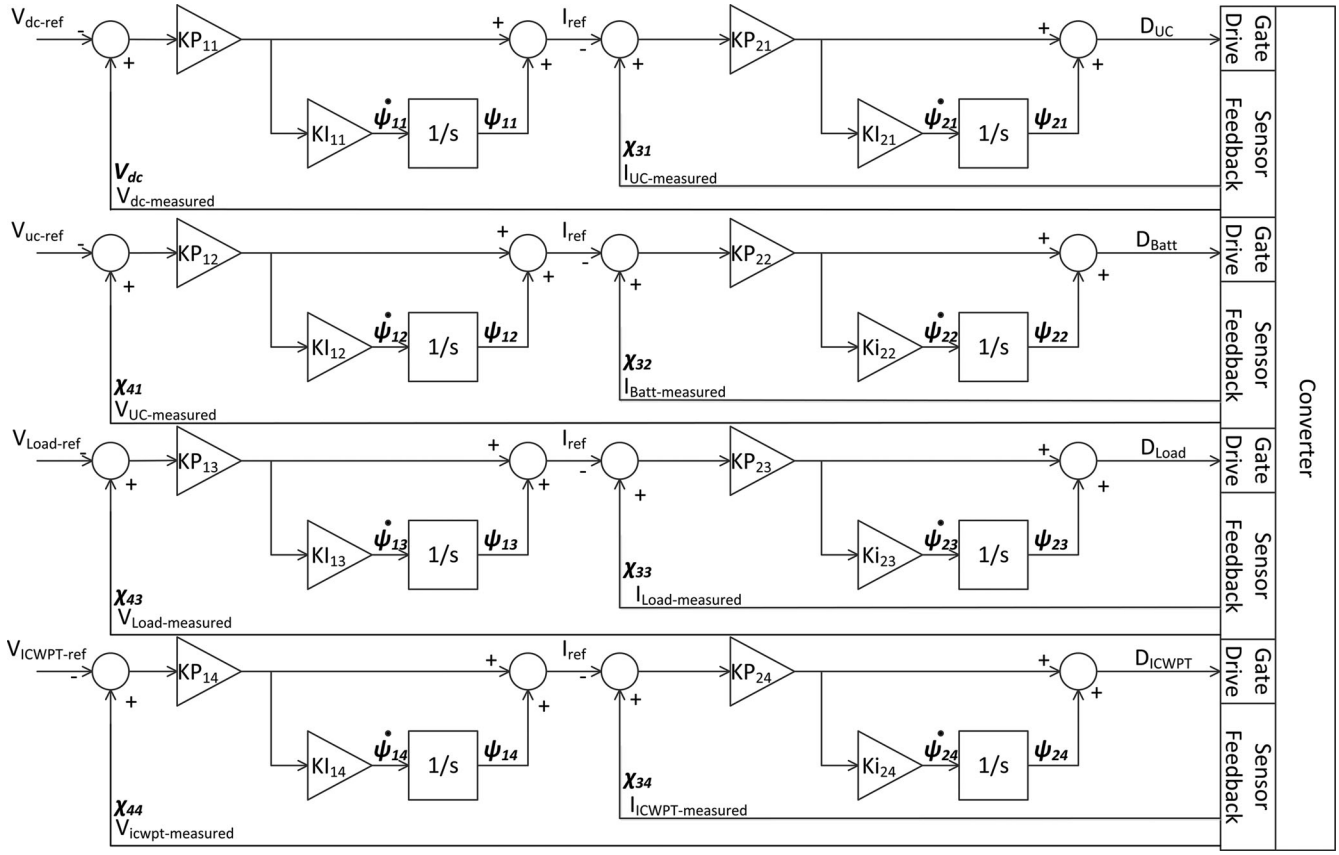

Fig. 7. Closed loop multiport controller for BEV MPEI.

TABLE III
POLE LOCATIONS FOR ON-BOARD MPEI SYSTEM

Pole #	$\hat{i}_{\rm load}=4$ $\hat{i}_{\rm icpt}=1.5$	$\hat{i}_{\rm load}=32$ $\hat{i}_{\rm icpt}=1.5$	$\hat{i}_{\rm load}=4$ $\hat{i}_{\rm icpt}=12$	$\hat{i}_{\rm load}=32$ $\hat{i}_{\rm icpt}=12$
		Poles		
1	-8.3×10^6	-8.3×10^6	-8.3×10^6	-8.3×10^6
2	-8.2×10^6	-8.2×10^6	-8.2×10^6	-8.2×10^6
3	-3.4×10^6	-3.4×10^6	-3.4×10^6	-3.4×10^6
4	-3.0×10^6	-3.0×10^6	-3.0×10^6	-3.0×10^6
5 & 6	-2.0×10^3	-2.0×10^3	-2.0×10^3	-2.0×10^3
7 & 8	-1.8×10^3	-1.8×10^3	-1.8×10^3	-1.8×10^3
8 & 10	-1.5×10^3	-1.5×10^3	-1.5×10^3	-1.5×10^3
11 & 12	-109 $\pm274j$	-109 $\pm274j$	-109 $\pm274j$	-109 $\pm274j$
13 & 14	-36.4	-36.4	-36.4	-36.4
15 & 16	$-0.202\pm$ $0.532j$	$-0.202\pm$ $0.532j$	$-0.202\pm$ $0.532j$	$-0.202\pm$ $0.532j$

B. Battery-UC Modeling Results

The battery-UC system was modeled according to the procedure in Section III-C. In order to model the Battery-UC system to ensure that the system is stable and that the battery does not have any high-frequency components, a load was added to the dc bus. The load is shown in Fig. 5 (labeled as $\hat{I}_{\rm DC}$ and $\Delta I_{\rm DC}$).

The system is now governed by the system of equations

$$\begin{aligned}\dot{x} &= Ax + Bu\\ y &= Cx\end{aligned} \tag{8}$$

where, x, B, and u are

$$x = [\psi_{11} \quad \psi_{21} \quad x_{31} \quad x_{41} \quad \psi_{12} \quad \psi_{22} \quad x_{32} \quad v_{dc}]' \tag{9}$$

$$B = \left[0 \quad 0 \quad 0 \quad 0 \quad 0 \quad 0 \quad 0 \quad \frac{1}{C_{dc}}\right]' \tag{10}$$

$$u = [i_{dc}]. \tag{11}$$

A is presented in (16) in the Appendix. In these equations, the Δ notation has been removed for convenience and any state variable is a small signal variable unless notated with the $\hat{}$ symbol. The poles for the Battery-UC only system are shown in Table II.

Since all the poles are on the left-half plane, the system is stable. In order to test the stability of the system further, the transient step response is shown in Fig. 6 (note the load is the current source $I_{\rm DC}$ shown in Fig. 5). Fig. 6(a) shows the small signal dc bus voltage fluctuation. Fig. 6(b) shows the battery current transient response. Note that the response time is on the order of seconds. Fig. 6(c) shows the UC current response and Fig. 6(d) shows the zoomed in view of the UC current to

highlight that the UC is providing the high-frequency response to the step change in the load current.

C. Complete Converter Modeling Results

Following the same procedure as Section IV-B, the control system of the entire BEV MPEI can be constructed. The control system is depicted in Fig. 7 and described in state space in

$$\dot{x} = Ax + Bu \tag{12}$$

$$A = \begin{bmatrix} A_{11} & A_{12} \\ A_{21} & A_{22} \end{bmatrix} \tag{13}$$

$$x = [\psi_{11} \quad \psi_{21} \quad x_{31} \quad x_{41} \quad \psi_{12} \quad \psi_{22} \quad x_{32} \quad v_{dc} \quad \psi_{13} \quad \psi_{23} \quad x_{33} \quad x_{43} \quad \psi_{14} \quad \psi_{24} \quad x_{34} \quad x_{44}]' \tag{14}$$

$$B = \left[0 \quad 0 \quad 0 \quad 0 \quad 0 \quad 0 \quad 0 \quad 0 \quad 0 \quad 0 \quad 0 \quad \frac{-1}{C_{\text{load}}} \quad 0 \quad 0 \quad 0 \quad \frac{-1}{C_{\text{wpt}}}\right]' \tag{15}$$

where A_{11}-A_{22} are given in the Appendix (17)–(20).

The poles of the system under various loading conditions are given in Table III. The poles of the system remain in the left-half plane and so the system remains stable even under widely varying operating conditions.

The step response to a two ampere step in ICPT current is given in Fig. 8. Similar to the Battery-UC case, the dc bus disturbance is minimal. Also, the UC responds on the order of 10 ms to bring the dc bus back into regulation while the battery current reaches maximum at around 7 s.

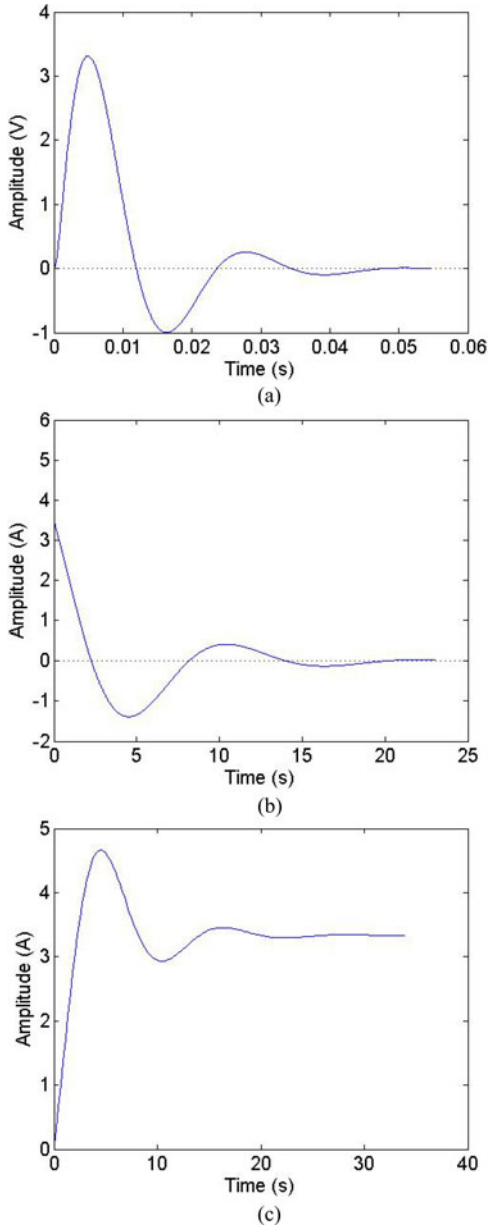

Fig. 8. Small signal model and simulation response to two ampere step in ICPT current. (a) Modeled DC bus voltage; (b) Modeled UC current; (c) Modeled battery current.

V. Experimental Results

An MPEI has been constructed with battery, UC, ICPT, and load terminals as shown in Fig. 9. The system has connection to an UC bank which has 9, 58-F, 16-V rated UC packs for a total of 6.44 F at 144 V when connected in series. The total energy capacity of the UC string is 18.5 Wh. The MPEI also has connection to 10, 12-V SLA batteries connected in series for a rated voltage of 120 V and a float voltage of up to 150 V. The total energy capacity is 2.16 kWh. The load consists of up to 15, 300-W light bulbs. Since the light bulbs are (almost) purely resistive, the power consumed by the load can be either adjusted in control by changing the output voltage reference or manually by adding or removing bulbs from the circuit. The ICPT system consists of two air core transceivers. The coupling factor is approximately 20%. The inner diameter of the concentration wound coils is 12 in and the air gap is 4 in. Each coil has 12 turns of two 13 AWG equivalent litz wires in parallel. The primary and secondary side inductance is 68 μH and the series compensation technique is used for both the primary and secondary sides (so the system is in a series–series configuration). TI's TMS320F28335 controlCARD is used to control the system. In this system, there are eight PWMs required and if the ICPT system was designed to be bidirectional, 12 PWMs would be necessary; which is the limit for this DSC. The switching frequency is 20 kHz. The primary side inverter is a simple full bridge inverter which is connected to a dc power supply and generates a square wave ac voltage waveform which is applied to the resonant circuit at the resonance frequency.

The ICPT was tested at various power levels as shown in Table IV. The efficiency was as high as 90% from dc input to dc output. When measuring efficiency the secondary side was rectified and applied directly to the light bulb resistors without any voltage regulation. A metal plate was added to examine the sensitivity of the system to foreign objects. The metal plate was 3.5 in from the primary transmitter and the efficiency dropped by only 3%. Transformer waveforms with the output rectified and filtered are given in Fig. 10. The resonant frequency is 100 kHz.

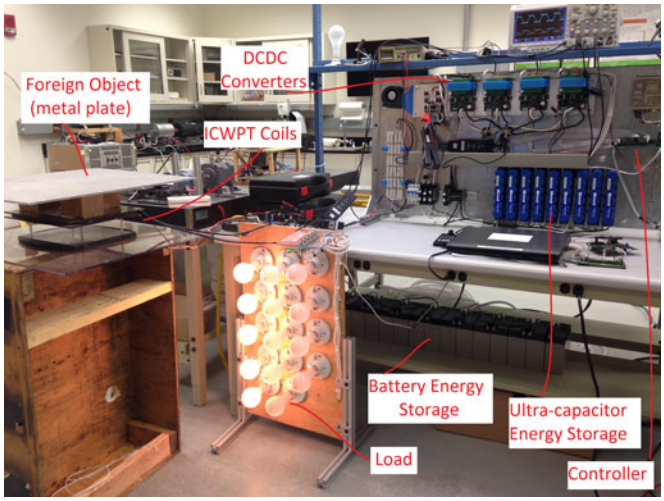

Fig. 9. Experimental testbed: ICPT capable MPEI system.

TABLE IV
EXPERIMENTAL EFFICIENCY OF ICPT

Power	Condition	DC Resistance	Efficiency
700 W	NA	7.23	64%
1100 W	NA	8.35	80%
1350 W	NA	11.75	86%
1500 W	NA	16.98	90%
1500 W	Metal Plate	17.55	87%

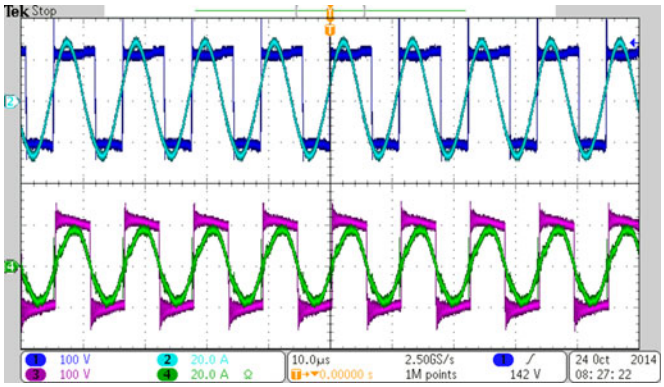

Fig. 10. Resonant transformer waveforms: Dark blue-Primary side voltage; Light blue- Primary side current; Magenta- Secondary side voltage; Green-Secondary side current.

One problem found with using light bulbs as a load is that the resistance changes significantly with the temperature of the light bulbs. Fig. 11 shows the response of the system when 160 W load is added to the system. It is apparent that the load is much larger at the instant of turn ON, so the load is actually quite harsher than a step function. In this test, the dc bus fluctuation was only 2.5 V (0.8% of the steady-state dc bus voltage). The key point to recognize is that the UC takes the high-frequency components by responding quickly to the load change, while the battery responds much slower without high-frequency components. Fig. 12 shows this more clearly when the negative step response is used by removing a 160 W load rather than adding

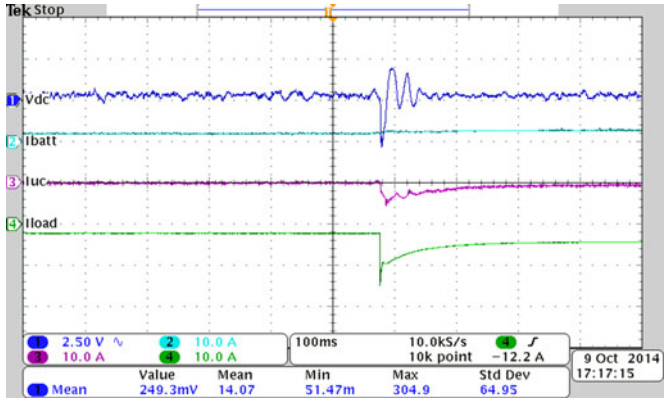

Fig. 11. Positive load current step response.

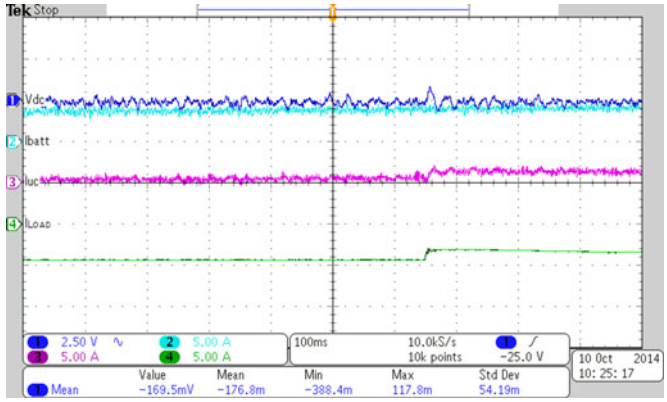

Fig. 12. Negative load current step response.

it. It is clear that the UCs respond much faster than the battery system (within 20 ms) and that the dc bus has little notification of the change of load.

While it is important to protect the batteries from high-frequency and high-magnitude currents coming from the load, it is even more important to protect the batteries from high-frequency and high-magnitude charging currents coming from the ICPT system. In a highway application, one can assume that the ICPT will be providing "pulse" power in short bursts. Therefore, the system will have many step inputs from the rising and falling edges of the pulse of power. Fig. 13 shows the response of the MPEI when the ICPT is suddenly turned ON. Similar to the load transient response, there is a transient appearing on the dc bus and the UC quickly takes the power; however, the battery current adjusts slowly over time.

Fig. 14 shows that over time with pulse charging the battery will begin to charge as the UC voltage rises above the reference voltage.

The loss of a source or load terminal is one key feature which was tested to show the utility of an MPEI-based system. Fig. 15 shows the transient response when there is a sudden loss of the battery converter. At $t \approx 16$ ms, the battery current is interrupted by a dc circuit breaker. The dc bus undergoes a fluctuation of approximately 5 V (1.7% of the steady-state dc bus voltage). The UC quickly begins to provide power for the load. They key

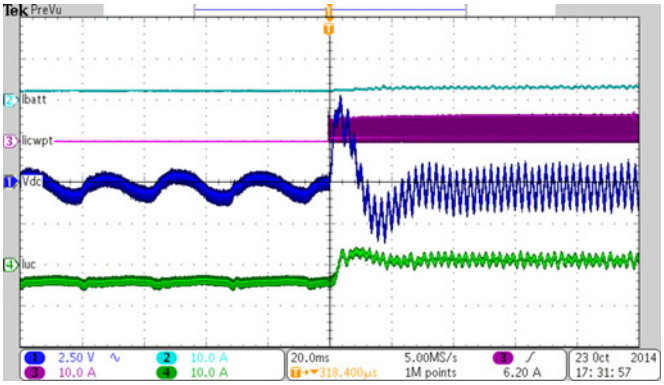

Fig. 13. DC bus transient due to ICPT pulse charging.

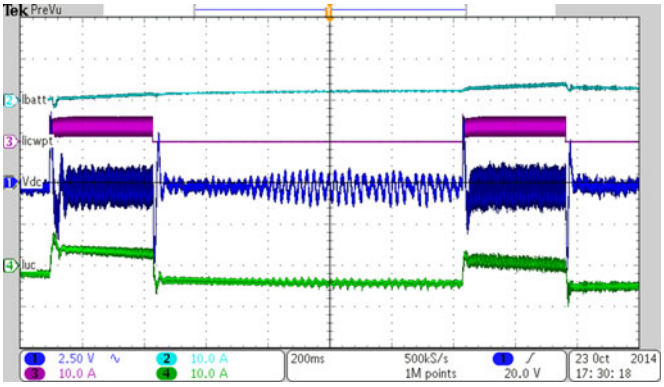

Fig. 14. ICPT pulse energy routing.

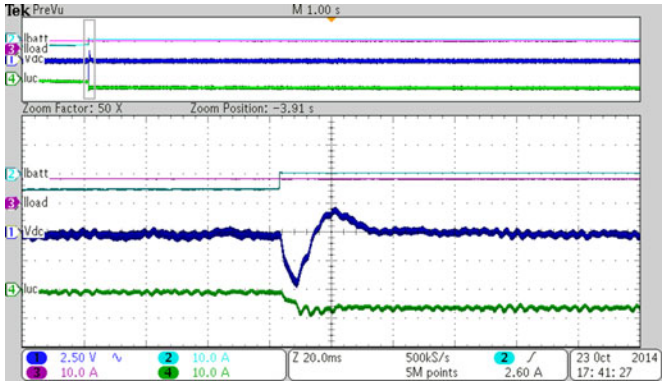

Fig. 15. Safety experiment: Loss of Battery.

point though is that the load terminal has no observable voltage or current fluctuations.

VI. Conclusion

An MPEI-based EV HESS was designed which serves as an energy router between various sources and sinks within an automobile. In this particular application, ICPT was used as the primary energy source. Meanwhile, batteries and UCs were used to provide power to the load. The batteries provided the low-frequency requirements, while the UCs provided the high-frequency and high-magnitude power. This was done by using a unique modeling and control approach that can be adapted to systems with different characteristics. With the MPEI and controller described, the UCs are responsible to maintaining

$$A = \begin{bmatrix} 0 & 0 & 0 & 0 & 0 & 0 & 0 & kp_{11}ki_{11} \\ -kp_{21}ki_{21} & 0 & kp_{21}ki_{21} & 0 & 0 & 0 & 0 & -kp_{11}kp_{21}ki_{21} \\ -\frac{\hat{V}_{\rm dc}kp_{21}}{L_1} & \frac{\hat{V}_{\rm dc}}{L_1} & \frac{\hat{V}_{\rm dc}kp_{21}}{L_1} & -\frac{1}{L_1} & 0 & 0 & 0 & \frac{\frac{V_{UC}}{\hat{V}_{\rm dc}}-kp_{11}kp_{21}\hat{V}_{\rm dc}}{L_1} \\ 0 & 0 & \frac{1}{C_{UC}} & 0 & 0 & 0 & 0 & 0 \\ 0 & 0 & 0 & kp_{12}ki_{12} & 0 & 0 & 0 & 0 \\ 0 & 0 & 0 & -kp_{12}kp_{22}ki_{22} & -kp_{22}ki_{22} & 0 & kp_{22}ki_{22} & 0 \\ 0 & 0 & 0 & \frac{-kp_{12}kp_{22}\hat{V}_{\rm dc}}{L_2} & -\frac{kp_{22}\hat{V}_{\rm dc}}{L_2} & \frac{\hat{V}_{\rm dc}}{L_2} & \frac{kp_{22}\hat{V}_{\rm dc}}{L_2} & \frac{V_{\rm batt}}{\hat{V}_{\rm dc}L_2} \\ \frac{kp_{21}\hat{x}_{31}}{C_{\rm dc}} & \frac{\hat{x}_{31}}{-C_{\rm dc}} & \frac{kp_{21}\hat{x}_{31}+\frac{V_{UC}}{\hat{V}_{\rm dc}}}{-C_{\rm dc}} & \frac{kp_{12}kp_{22}\hat{x}_{32}}{C_{\rm dc}} & \frac{kp_{22}\hat{x}_{32}}{C_{\rm dc}} & \frac{\hat{x}_{32}}{-C_{\rm dc}} & \frac{kp_{22}\hat{x}_{32}+\frac{V_{\rm batt}}{\hat{V}_{\rm dc}}}{-C_{\rm dc}} & \frac{kp_{11}kp_{21}\hat{x}_{31}}{C_{\rm dc}} \end{bmatrix} \quad (16)$$

$$A_{11} = \begin{bmatrix} 0 & 0 & 0 & 0 & 0 & 0 & 0 & kp_{11}ki_{11} \\ -kp_{21}ki_{21} & 0 & kp_{21}ki_{21} & 0 & 0 & 0 & 0 & -kp_{11}kp_{21}ki_{21} \\ -\frac{\hat{V}_{\rm dc}kp_{21}}{L_1} & \frac{\hat{V}_{\rm dc}}{L_1} & \frac{\hat{V}_{\rm dc}kp_{21}}{L_1} & -\frac{1}{L_1} & 0 & 0 & 0 & \frac{\frac{V_{UC}}{\hat{V}_{\rm dc}}-kp_{11}kp_{21}\hat{V}_{\rm dc}}{L_1} \\ 0 & 0 & \frac{1}{C_{UC}} & 0 & 0 & 0 & 0 & 0 \\ 0 & 0 & 0 & kp_{12}ki_{12} & 0 & 0 & 0 & 0 \\ 0 & 0 & 0 & -kp_{12}kp_{22}ki_{22} & -kp_{22}ki_{22} & 0 & kp_{22}ki_{22} & 0 \\ 0 & 0 & 0 & \frac{-kp_{12}kp_{22}\hat{V}_{\rm dc}}{L_2} & -\frac{kp_{22}\hat{V}_{\rm dc}}{L_2} & \frac{\hat{V}_{\rm dc}}{L_2} & \frac{kp_{22}\hat{V}_{\rm dc}}{L_2} & \frac{V_{\rm batt}}{\hat{V}_{\rm dc}L_2} \\ \frac{kp_{21}\hat{x}_{31}}{C_{\rm dc}} & \frac{\hat{x}_{31}}{-C_{\rm dc}} & \frac{kp_{21}\hat{x}_{31}+\frac{V_{UC}}{\hat{V}_{\rm dc}}}{-C_{\rm dc}} & \frac{kp_{12}kp_{22}\hat{x}_{32}}{C_{\rm dc}} & \frac{kp_{22}\hat{x}_{32}}{C_{\rm dc}} & \frac{\hat{x}_{32}}{-C_{\rm dc}} & \frac{kp_{22}\hat{x}_{32}+\frac{V_{\rm batt}}{\hat{V}_{\rm dc}}}{-C_{\rm dc}} & \frac{kp_{11}kp_{21}\hat{x}_{31}}{C_{\rm dc}} \end{bmatrix} \quad (17)$$

$$A_{12} = \begin{bmatrix} 0 & 0 & 0 & 0 & 0 & 0 & 0 & 0 \\ 0 & 0 & 0 & 0 & 0 & 0 & 0 & 0 \\ 0 & 0 & 0 & 0 & 0 & 0 & 0 & 0 \\ 0 & 0 & 0 & 0 & 0 & 0 & 0 & 0 \\ 0 & 0 & 0 & 0 & 0 & 0 & 0 & 0 \\ 0 & 0 & 0 & 0 & 0 & 0 & 0 & 0 \\ 0 & 0 & 0 & 0 & 0 & 0 & 0 & 0 \\ \frac{kp_{23}\hat{x}_{33}}{C_{\mathrm{dc}}} & \frac{\hat{x}_{33}}{C_{\mathrm{dc}}} & \frac{kp_{23}\hat{x}_{33}+\frac{V_{load}}{\hat{V}_{\mathrm{dc}}}}{C_{\mathrm{dc}}} & \frac{kp_{13}kp_{23}\hat{x}_{33}}{C_{\mathrm{dc}}} & \frac{kp_{24}\hat{x}_{34}}{C_{\mathrm{dc}}} & \frac{\hat{x}_{34}}{C_{\mathrm{dc}}} & \frac{kp_{24}\hat{x}_{34}+\frac{V_{\mathrm{icwpt}}}{\hat{V}_{\mathrm{dc}}}}{C_{\mathrm{dc}}} & \frac{kp_{14}kp_{24}\hat{x}_{34}}{C_{\mathrm{dc}}} \end{bmatrix} \tag{18}$$

$$A_{21} = \begin{bmatrix} 0 & 0 & 0 & 0 & 0 & 0 & 0 & 0 \\ 0 & 0 & 0 & 0 & 0 & 0 & 0 & 0 \\ 0 & 0 & 0 & 0 & 0 & 0 & 0 & \frac{V_{load}}{\hat{V}_{\mathrm{dc}}L_3} \\ 0 & 0 & 0 & 0 & 0 & 0 & 0 & 0 \\ 0 & 0 & 0 & 0 & 0 & 0 & 0 & 0 \\ 0 & 0 & 0 & 0 & 0 & 0 & 0 & 0 \\ 0 & 0 & 0 & 0 & 0 & 0 & 0 & \frac{V_{\mathrm{wpt}}}{\hat{V}_{\mathrm{dc}}L_4} \\ 0 & 0 & 0 & 0 & 0 & 0 & 0 & 0 \end{bmatrix} \tag{19}$$

$$A_{22} = \begin{bmatrix} 0 & 0 & 0 & kp_{13}ki_{13} & 0 & 0 & 0 & 0 \\ -kp_{23}ki_{23} & 0 & kp_{23}ki_{23} & -kp_{13}kp_{23}ki_{23} & 0 & 0 & 0 & 0 \\ -\frac{kp_{23}\hat{V}_{\mathrm{dc}}}{L_3} & \frac{\hat{V}_{\mathrm{dc}}}{L_3} & \frac{\hat{V}_{\mathrm{dc}}kp_{23}}{L_3} & -\frac{1+kp_{13}kp_{23}\hat{V}_{\mathrm{dc}}}{L_3} & 0 & 0 & 0 & 0 \\ 0 & \frac{1}{C_{\mathrm{load}}} & 0 & 0 & 0 & 0 & 0 & 0 \\ 0 & 0 & 0 & 0 & 0 & 0 & 0 & kp_{14}ki_{14} \\ 0 & 0 & 0 & 0 & -kp_{24}ki_{24} & 0 & kp_{24}ki_{24} & -kp_{14}kp_{24}ki_{24} \\ 0 & 0 & 0 & 0 & \frac{kp_{24}\hat{V}_{\mathrm{dc}}}{L_4} & \frac{\hat{V}_{\mathrm{dc}}}{L_4} & \frac{kp_{24}\hat{V}_{\mathrm{dc}}}{L_4} & -\frac{1+kp_{14}kp_{24}\hat{V}_{\mathrm{dc}}}{L_4} \\ 0 & 0 & 0 & 0 & 0 & 0 & \frac{1}{C_{\mathrm{icwpt})}} & 0 \end{bmatrix}. \tag{20}$$

the dc bus (and thus providing power to the load or absorbing power from the ICPT system) and the batteries are responsible for maintaining the SoC of the UCs. In this way, the stability of the entire system can be studied, including SoC of the UCs. Stability can be ensured while also protecting the battery from high-frequency and high-magnitude current. The ICPT terminal is shown to be capable of 90+% efficiency from the dc bus of the primary side inverter to the dc bus of the MPEI. Assuming reasonable dc–dc converter efficiency, the efficiency from input to load can be as high as 85% or better. This is a substantial improvement over internal combustion vehicles and eliminates the range anxiety of traditional BEVs.

Appendix
State Space Equations for MPEI

See equations (16) and (17) shown at the bottom of the previous page and equations (18), (19), and (20) shown at the top of the page.

Acknowledgment

The author would like to thank Professor B. Fahimi for his financial and intellectual support in this endeavor.

References

[1] D. Simmons. (2012). "Hard facts: An energy primer," The Institute for Energy Research. [Online]. Available: http://instituteforenergyresearch.org/media/hardfacts.pdf

[2] J. Hearron, M. McDonough, A. Ranjbar, W. Wang, C. Lin, P. Shamsi, S. Manohar, and B. Fahimi, "The sustainability of new technologies in vehicular transportation," in *Proc. IEEE Vehicle Power Propulsion Conf.*, Sep. 2011, pp. 1–6.

[3] Y. Xiao, C. Lin, and B. Fahimi, "Online state of charge estimation in electrochemical batteries: Application of pattern recognition techniques," in *Proc. IEEE 28th Annu. Appl. Power Electron. Conf. Expo.*, Mar. 2013, pp. 2474–2478.

[4] F. T. Wagner, B. Lakshmanan, and M. F. Mathias, "Electrochemistry and the future of the automobile," *J. Phys. Chem. Lett.*, vol. 1, no. 14, pp. 2204–2219, 2010.

[5] M. Whittingham, "History, evolution, and future status of energy storage," *Proc. IEEE*, vol. 100, pp. 1518–1534, May 2012.

[6] X. Wu, T. Maeda, H. Fujimoto, S. Ishii, and K. Fujita, "Three-phase high frequency transformer isolated AC to DC converter for EV battery quick charging," in *Proc. 7th Int. Power Electron. Motion Control Conf.*, Jun. 2012, vol. 1, pp. 643–647.
[7] S.-H. Han, M.-G. Jeong, S.-K. Yang, and H.-B. Lee, "Performance test for EV quick charger," in *Proc. IEEE Veh. Power Propulsion Conf.*, Oct. 2012, pp. 1516–1519.
[8] I. Martin, T. Markel, and J. Sanz, "New task on quick charging technology of electric vehicles in IEA IA-HEV (hybrid and electric vehicles)," in *Proc. World Electric Veh. Symp. Exhib.*, Nov. 2013, pp. 1–5.
[9] G. Nagendra, J. Boys, G. Covic, B. Riar, and A. Sondhi, "Design of a double coupled IPT EV highway," in *Proc. IECON 39th Annu. Conf. IEEE Ind. Electron. Soc.*, Nov. 2013, pp. 4606–4611.
[10] M. McDonough, P. Shamsi, and B. Fahimi, "Application of multi-port power electronic interface for contactless transfer of energy in automotive applications," in *Proc. IEEE Veh. Power Propulsion Conf.*, Sep. 2011, pp. 1–6.
[11] O. C. Onar, J. M. Miller, S. L. Campbell, C. Coomer, C. White, and L. E. Seiber, "A novel wireless power transfer for in-motion ev/phev charging," in *Proc. IEEE 28th Annu. Appl. Power Electron. Conf. Expo.*, Mar. 2013, pp. 3073–3080.
[12] B. Song, J. Shin, S. Chung, S. Shin, S. Lee, Y. Kim, G. Jung, and S. Jeon, "Design of a pickup with compensation winding for on-line electric vehicle (OLEV)," in *Proc. IEEE Wireless Power Transfer*, May 2013, pp. 60–62.
[13] "Hevo power: Wireless charging for electric vehicles," (2014). [Online]. Available: http://hevopower.com/
[14] "Witricity: Automotive," (2014). [Online]. Available: http://witricity.com/applications/automotive/
[15] C. Hochgraf, J. Basco, T. Bohn, and I. Bloom, "Effect of ultracapacitor-modified PHEV protocol on performance degradation in lithium-ion cells." *J. Power Sources*, vol. 246, pp. 965–969, Sep. 2012.
[16] A. Jossen, V. Spath, H. Doring, and J. Garche, "Battery management systems (BMS) for increasing battery life time," in *Proc. 21st Int. Telecommun. Energy Conf.*, Jun 1999, p. 6.
[17] B. Vulturescu, S. Butterbach, C. Forgez, G. Coquery, and G. Friedrich, "Ageing study of a supercapacitor-battery storage system," in *Proc. XIX Int. Conf. Electr. Mach.*, Sep. 2010, pp. 1–6.
[18] A. Ostadrahimi and A. Radan, "Utilization of interleaved converter to improve battery performance in electric and electrical hybrid vehicles," in *Proc. 5th Power Electron., Drive Syst. Technol. Conf.*, Feb. 2014, pp. 624–628.
[19] K. Qian, C. Zhou, Y. Yuan, and M. Allan, "Temperature effect on electric vehicle battery cycle life in vehicle-to-grid applications," in *Proc. Electr. Distrib.*, Sep. 2010, pp. 1–6.
[20] A. Gee and R. Dunn, "Novel battery/supercapacitor hybrid energy storage control strategy for battery life extension in isolated wind energy conversion systems," in *Proc. 45th Int. Univ. Power Eng. Conf.*, Aug. 2010, pp. 1–6.
[21] J. Miller, P. McCleer, M. Everett, and E. Strangas, "Ultracapacitor plus battery energy storage system sizing methodology for HEV power split electronic CVT's," in *Proc. IEEE Int. Symp. Ind. Electron.*, Jun. 2005, vol. 1, pp. 317–324.
[22] B. Chen, Y. Gao, M. Ehsani, and J. Miller, "Design and control of a ultracapacitor boosted hybrid fuel cell vehicle," in *Proc. IEEE Veh. Power Propulsion Conf.*, Sep. 2009, pp. 696–703.
[23] J. Miller and R. Smith, "Ultra-capacitor assisted electric drives for transportation," in *Proc. IEEE Int. Electr. Mach. Drives Conf.*, Jun. 2003, vol. 2, pp. 670–676.
[24] J. Cao and A. Emadi, "A new battery/ultracapacitor hybrid energy storage system for electric, hybrid, and plug-in hybrid electric vehicles," *IEEE Trans. Power Electron.*, vol. 27, no. 1, pp. 122–132, Jan. 2012.
[25] A. Khaligh and Z. Li, "Battery, ultracapacitor, fuel cell, and hybrid energy storage systems for electric, hybrid electric, fuel cell, and plug-in hybrid electric vehicles: State of the art," *IEEE Trans. Veh. Technol.*, vol. 59, no. 6, pp. 2806–2814, Jul. 2010.
[26] S. Falcones, R. Ayyanar, and X. Mao, "A DC DC multiport-converter-based solid-state transformer integrating distributed generation and storage," *IEEE Trans. Power Electron.*, vol. 28, no. 5, pp. 2192–2203, May 2013.
[27] Z. Ding, C. Yang, Z. Zhang, C. Wang, and S. Xie, "A novel soft-switching multiport bidirectional DC DC converter for hybrid energy storage system," *IEEE Trans. Power Electronics*, vol. 29, no. 4, pp. 1595–1609, Apr. 2014.
[28] S. Rezaee and E. Farjah, "A dc dc multiport module for integrating plug-in electric vehicles in a parking lot: Topology and operation," *IEEE Trans. Power Electron.*, vol. 29, no. 11, pp. 5688–5695, Nov. 2014.
[29] H. Wu, J. Zhang, and Y. Xing, "A family of multiport buck boost converters based on dc-link-inductors (DLIS)," *IEEE Trans. Power Electron.*, vol. 30, no. 2, pp. 735–746, Feb. 2015.
[30] Y. Zhang, Z. Jiang, and X. Yu, "Control strategies for battery/supercapacitor hybrid energy storage systems," in *Proc. IEEE Energy 2030 Conf.*, Nov. 2008, pp. 1–6.
[31] J. Miller, O. Onar, C. White, S. Campbell, C. Coomer, L. Seiber, R. Sepe, and A. Steyerl, "Demonstrating dynamic wireless charging of an electric vehicle: The benefit of electrochemical capacitor smoothing," *IEEE Power Electron. Mag.*, vol. 1, no. 1, pp. 12–24, Mar. 2014.
[32] M. Ortuzar, J. Moreno, and J. Dixon, "Ultracapacitor-based auxiliary energy system for an electric vehicle: Implementation and evaluation," *IEEE Trans. Ind. Electron.*, vol. 54, no. 4, pp. 2147–2156, Aug. 2007.
[33] P. Shamsi and B. Fahimi, "Modeling of a 3-phase multi-port power electronic interface," in *Proc. IEEE Int. Symp. Ind. Electron.*, May 2012, pp. 1035–1039.
[34] P. Shamsi, "Stability assessment of a multi-port power electronic interface for hybrid micro-grid applictions," Ph.D. dissertation, The Univ. of Texas at Dallas, TX, USA, Dec. 2012.
[35] M. McDonough, "A multi-port power electronics interface for battery powered electric vehicles: Application of inductively coupled wireless power transfer and hybrid energy storage system," Ph.D. dissertation, The Univ. Texas at Dallas, TX, USA, Dec. 2014.
[36] M. McDonough, P. Shamsi, and B. Fahimi, "Dynamic modeling of ICPT considering misalignment and speed of vehicle," in *Proc. IEEE Veh. Power Propulsion Conf.*, Sep. 2011, pp. 1–6.
[37] S. Sanders, J. Noworolski, X. Liu, and G. C. Verghese, "Generalized averaging method for power conversion circuits," *IEEE Trans. Power Electron.*, vol. 6, no. 2, pp. 251–259, Apr. 1991.

Matthew K. McDonough was born on August 27, 1987, and grew up in the town of Blum, TX, USA. He received the Bachelor's of Science degree in electrical engineering from The University of Texas at Arlington, Arlington, TX, in May 2010, and the Ph.D. degree from The University of Texas at Dallas, TX, in December 2014.

He joined the Renewable Energy and Vehicular Technology Laboratory in Arlington and later moved with the lab to The University of Texas at Dallas in the Fall of 2010. His primary research interests include application of renewable energy resources. Specifically, he is interested in microgrids, dc–dc converters, integration of wide band-gap devices, dc–ac and ac–dc converters, multiport converters, and transportation technology.